International Journal of Modern Physics A
Vol. 26, Nos. 10 & 11 (2011) 1807–1821

DOI: 10.1142/S0217751X11053201

World Scientific
www.worldscientific.com

HIGH-ORDER OUT-OF-PLANE EXPANSION FOR 3D FIELDS

K. MAKINO* and M. BERZ
Department of Physics and Astronomy, Michigan State University, East Lansing, MI 48824, USA
**makino@msu.edu*

C. JOHNSTONE
Fermilab, Batavia, IL 60510, USA

The precise determination of the dynamics in accelerators with complicated field arrangements such as Fixed Field Alternating Gradient accelerators (FFAG) depends critically on the ability to describe the appearing magnetic fields in full 3D. However, frequently measurements or models of FFAG fields postulate their behavior in the midplane only, and rely on the fact that this midplane field and its derivatives determine the field in all of space. The detailed knowledge of the resulting out-of-plane fields is critical for a careful assessment of the vertical dynamics.

We describe a method based on the differential algebraic (DA) approach to obtain the resulting out-of-plane expansions to any order in an order-independent, straightforward fashion. In particular, the resulting fields satisfy Maxwell's equations to the order of the expansion up to machine precision errors, and without any inaccuracies that can arise from conventional divided difference or finite element schemes for the computation of out-of-plane fields.

The method relies on re-writing the underlying PDE as a fixed point problem involving DA operations, and in particular the differential algebraic integration operator. We illustrate the performance of the method for a variety of practical examples, and obtain estimates for the orders necessary to describe the fields to a prescribed accuracy.

1. Introduction

The differential algebraic (DA) methods[1,2] allow the efficient computation and manipulation of high-order Taylor transfer maps. When integrating transfer maps through electromagnetic fields, the full 3D fields are computed as part of each integration time step using DA PDE (partial differential equation) solvers. First, we address the mechanism of the method of DA fixed point PDE solvers, and as will be seen, the method is very compact and fast, and only requires an analytic representation of the field in the midplane.

Compared to multipole electromagnetic elements such as dipoles, quadrupoles and so forth, the fringe fields in FFAGs and related accelerators are dominating and extend for relatively long distance. After developing the theoretical background, we study the practical performance of the method to illustrate the quality of the

out-of-plane expansions for various examples, including a model of a dipole field with known 3D field, as well as models of FFAG fringe fields based on Enge function field falloff as implemented in the FFAG simulation tool FACT Particularly because of this long extension of the fringe fields, in practice it is important to be able to efficiently combine the fields of all poles together, and then hand the total midplane field to the DA PDE solvers.

2. High-Order Derivatives of Fields

The idea of differential algebraic (DA) methods[1–3] is based on the observation that it is possible to extract more information about a function than its mere values on computers. One can introduce an operation T denoting the extraction of the Taylor coefficients of a pre-specified order n of the function $f \in C^n(R^v)$. In mathematical terms, T is an equivalence relation, and the application of T corresponds to the transition from the function f to the equivalence class $[f]$ comprising all those functions with identical Taylor expansion in v variables to order n; the classes are apparently characterized by the collection of Taylor coefficients. Since Taylor coefficients of order n for sums and products of functions as well as scalar products with reals can be computed from those of the summands and factors, the set of equivalence classes of functions can be endowed with well-defined operations, leading to the so-called Truncated Power Series Algebra (TPSA).[4,5] More advanced tools address the composition of functions, their inversion, solutions of implicit equations, and the introduction of common elementary functions.[1] For treatment of ODEs and PDEs, the power of TPSA can be enhanced by the introduction of derivations ∂ and their inverses ∂^{-1}, corresponding to the differentiation and integration on the space of functions, resulting in the Differential Algebra ${}_nD_v$. This structure allows the direct treatment of many questions connected with differentiation and integration of functions, including the solution of the ODEs $d\vec{x}/dt = \vec{f}(\vec{x}, t)$ describing the motion and PDEs describing the fields,[6–8] and will be the key ingredient for the computation of out-of-plane fields as discussed in the next section.

High-order out-of-plane expansions can be done via recursion formulas (see Refs. 1, 9–11 and references therein) and require the higher derivatives of the field falloff. One of the simplest applications of the DA method is to compute these derivatives accurately. To illustrate the behavior of the method of computing derivatives of very high orders, we show the results of the computation of one-dimensional derivatives of a common ingredient in the analytic description of the falloff of midplane fields in the vicinity of the edge of the magnet, the so-called Enge function

$$E(s) = \frac{1}{1 + \exp(a_0 + a_1(s/d) + ... + a_k(s/d)^k}, \tag{1}$$

where s is the distance to the magnet, the coefficients a_0 to a_k describe the shape of the falloff, and the d is a scaling factor describing the half gap of the magnet

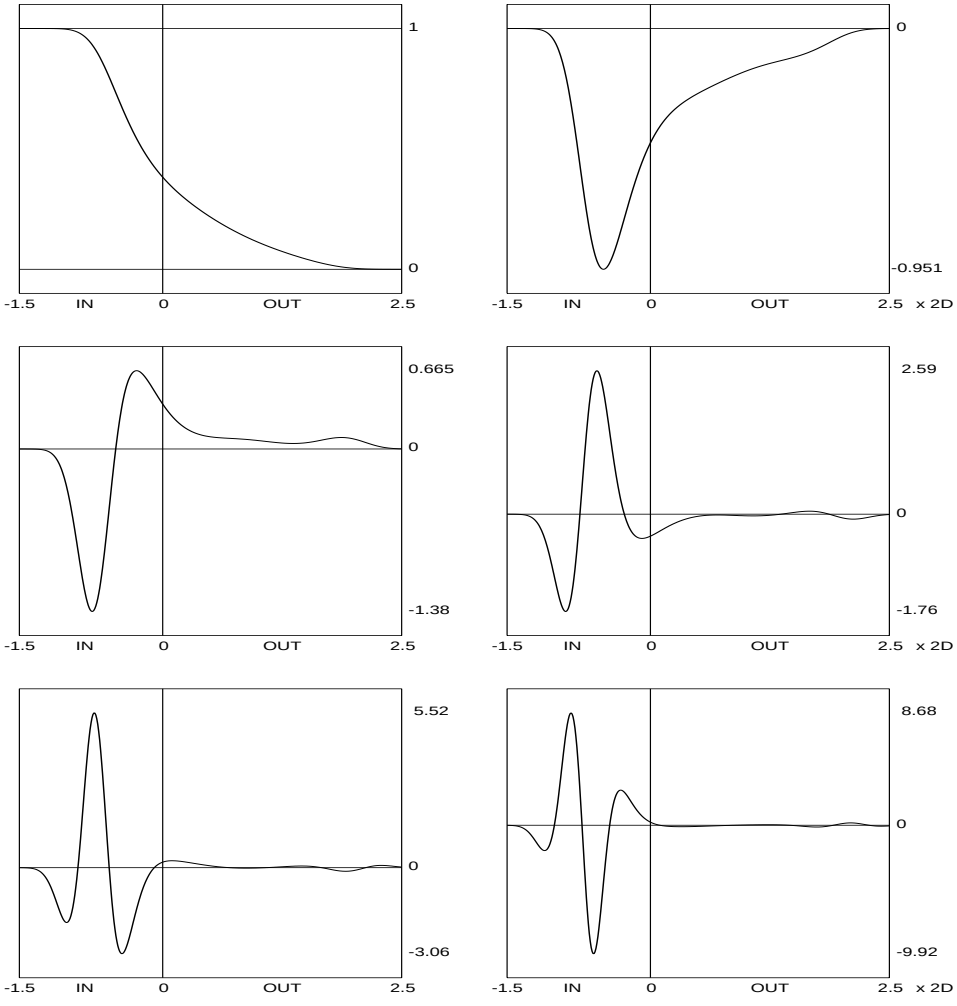

Fig. 1. Fringe field falloff profile of the COSY default model for magnetic dipoles, and derivatives 1 through 5.

at the edge. The code COSY INFINITY contains a library of default coefficients for common particle optical elements,[12] but for specific devices, it is important to determine the most suitable values of the coefficients.

In order to determine the high-order derivatives of the Enge function necessary for the out-of-plane expansion discussed later, it is merely required to evaluate the expression of the Enge function (1) using DA arithmetic with the variable s being one of the DA variables. To illustrate this feature, we show the field falloff profile of the default model for magnetic quadrupoles in COSY INFINITY, and their derivatives up to order five in Fig. 1, and to show that the orders do not represent a limitation, orders 10, 20, and 30 in Fig. 2.

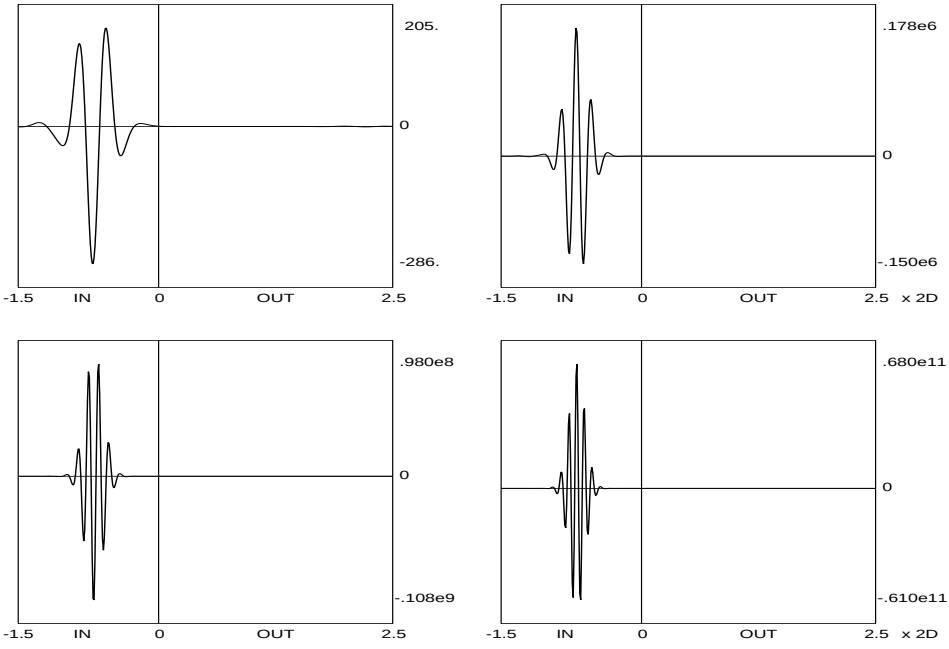

Fig. 2. Fringe field falloff of the COSY default model for magnetic dipoles, derivatives 10, 20, 30, and 40.

The figures illustrate the ease with which it is possible to obtain derivatives to very high orders using DA methods. Furthermore, different from conventional numerical differentiation schemes, the values are accurate to mere round-off error and are close to machine precision, which manifests itself in the absence of any apparent noise in the representation of the higher derivatives.

3. DA Fixed Point PDE Solvers

As discussed in the previous section, for the treatment of ODEs and PDEs, the power of TPSA can benefits from the introduction of derivations ∂ and their inverses ∂^{-1}, corresponding to the differentiation and integration on the space of functions, resulting in the Differential Algebra ${}_nD_v$. This structure allows the direct treatment of many questions connected with differentiation and integration of functions, including the solution of the ODEs $d\vec{x}/dt = \vec{f}(\vec{x}, t)$ describing the motion and PDEs describing the fields.[3]

For any element $[f] \in {}_nD_v$ we define the depth $\lambda([f])$ as

$$\lambda([f]) = \begin{cases} \text{Order of the first nonvanishing derivative of } f & \text{if } [f] \neq 0 \\ n+1 & \text{if } [f] = 0 \end{cases}.$$

In particular, any function f that does not vanish at the origin has $\lambda([f]) = 0$.

Let $\mathcal{O}$ be an operator on the set $M \subset {}_nD_v^m$, where ${}_nD_v^m$ is the set describing vector functions $\vec{f} = (f_1, ..., f_m)$ from R^v to R^m. Then we say that $\mathcal{O}$ is contracting on M if for any $\vec{a}$, $\vec{b} \in M$ with $\vec{a} \neq \vec{b}$,

$$\lambda(\mathcal{O}(\vec{a}) - \mathcal{O}(\vec{b})) > \lambda(\vec{a} - \vec{b}).$$

In practical terms this means that after application of $\mathcal{O}$, the derivatives in $\vec{a}$ and $\vec{b}$ agree to a higher order than before application of $\mathcal{O}$. For example, the anti-derivation ∂_k^{-1} is a contracting operator. Contracting operators satisfy a fixed point theorem:

Theorem 3.1. *(DA Fixed Point Theorem) Let $\mathcal{O}$ be a contracting operator on $M \subset {}_nD_v$ that maps M into M. Then $\mathcal{O}$ has a unique fixed point $a \in M$ that satisfies the fixed point problem $a = \mathcal{O}(a)$. Moreover, let a_0 be any element in M. Then the sequence $a_k = \mathcal{O}(a_{k-1})$ for $k = 1, 2, ...$ converges in finitely many steps (in fact, at most $(n + 1)$ steps) to the fixed point a.*

The fixed point theorem is of great practical usefulness since it assures the existence of a solution, and moreover allows its exact determination in a very simple way in finitely many steps. The proof of the theorem can be found in.[1] The DA fixed point theorem has many useful applications, in particular a rather straightforward solution of ODEs and PDEs.[3]

The direct availability of the derivation ∂ and its inverse ∂^{-1} allows to devise efficient numerical PDE solvers of any order. The DA fixed point theorem allows one to solve PDEs iteratively in finitely many steps by rephrasing them in terms of a fixed point problem. The details depend on the PDE at hand, but the key idea is to eliminate differentiation with respect to one variable and replace it by integration. As an example, consider a rather general PDE

$$a_1 \frac{\partial}{\partial x}\left(a_2 \frac{\partial}{\partial x} V\right) + b_1 \frac{\partial}{\partial y}\left(b_2 \frac{\partial}{\partial y} V\right) + c_1 \frac{\partial}{\partial z}\left(c_2 \frac{\partial}{\partial z} V\right) = 0,$$

where a_1, a_2, b_1, b_2, c_1 c_2 are functions of x, y, z. The PDE is re-written as

$$V = V|_{y=0} + \int_0^y \frac{1}{b_2}\left\{\left(b_2 \frac{\partial V}{\partial y}\right)\Big|_{y=0} - \int_0^y \left[\frac{a_1}{b_1}\frac{\partial}{\partial x}\left(a_2 \frac{\partial V}{\partial x}\right) + \frac{c_1}{b_1}\frac{\partial}{\partial z}\left(c_2 \frac{\partial V}{\partial z}\right)\right] dy\right\} dy\,.$$

The equation is now in fixed point form. Now assume the derivatives of V and $\partial V/\partial y$ with respect to x and z are known in the plane $y = 0$. If the right hand side is contracting with respect to y, the various orders in y can be calculated by mere iteration.

As a particularly important example, consider the Laplace equation. It can be represented in general curvilinear coordinates.[6,8] In the special case of a curvilinear coordinate system, the Laplace equation is obtained as[6,8]

$$\triangle V = \frac{1}{1+hx}\frac{\partial}{\partial x}\left[(1+hx)\frac{\partial V}{\partial x}\right] + \frac{\partial^2 V}{\partial y^2} + \frac{1}{1+hx}\frac{\partial}{\partial s}\left(\frac{1}{1+hx}\frac{\partial V}{\partial s}\right) = 0.$$

In the case of a straight section, where $h = 0$, it reduces to nothing but the Cartesian Laplace equation. The fixed point form of the Laplace equation in the planar curvilinear coordinates is

$$V = V|_{y=0} + \int_0^y \left(\frac{\partial V}{\partial y}\right)\Big|_{y=0} dy - \int_0^y \int_0^y \left\{ \frac{1}{1+hx} \frac{\partial}{\partial x} \left[(1+hx) \frac{\partial V}{\partial x} \right] + \frac{1}{1+hx} \frac{\partial}{\partial s} \left(\frac{1}{1+hx} \frac{\partial V}{\partial s} \right) \right\} dy dy \,.$$

In this form, the right hand side has the interesting property that, regardless of what function V is inserted, the parts not depending on y are reproduced exactly, since all integrals introduce y dependence. Because of the integral operation, for a given choice of x and s and considering only the y dependence, the right hand side is contracting. In COSY INFINITY,[13] the planar curvilinear Laplace equation is solved by the following very compact code:

```
POLD := P ;

HF := 1+H{*}DA(IX) ; HI := 1/HF ;

LOOP I 2 NOC+2 2 ;

P := POLD - INTEG(IY,INTEG(IY, HI{*}( DER(IX,HF{*}DER(IX,P))

+ DER(IS,HI{*}DER(IS,P)) ) )) ;

ENDLOOP ;
```

Here the boundary condition $V|_{y=0} + \int_0^y (\partial V/\partial y)|_{y=0}\, dy$ is provided through the incoming form of `P`, which is obtained using the DA expression in COSY. The DA fixed point iteration converges to the solution potential `P` in finitely many steps. `DA(IX)` represents the identity for x, `NOC` is the current transfer map computation order, and `DER(I,...)` and `INTEG(I,...)` correspond to the DA derivative and the DA anti-derivative operations with respect to the variable specified by the first argument `I`, namely "∂_{x_I}" and "$\int_0^{x_I} dx_I$". The full 3D field is derived from the solution potential `P`, using the elementary DA derivations ∂_x, ∂_y and ∂_s. In coded form, we have

```
BX := DER(IX,P) ; BY := DER(IY,P) ; BZ := DER(IS,P);
```

The advantages of the method are:

- only the field in the midplane is needed;
- the resulting field will always satisfy the stationary Maxwell equations;
- the method works to any order.

Although this is not of primary interest for the computation of fields of FFAGs, we briefly also discuss another important coordinate system, the cylindrical coordinates, in which the Laplace equation takes the simple form

$$\triangle V = \frac{1}{r}\frac{\partial}{\partial r}\left(r\frac{\partial V}{\partial r}\right) + \frac{1}{r^2}\frac{\partial^2 V}{\partial \phi^2} + \frac{\partial^2 V}{\partial s^2} = 0.$$

If V does not depend on ϕ, namely V is rotationally symmetric, as in solenoid magnets, the fixed point form of the Laplace equation is simplified to

$$V = V|_{r=0} - \int_0^r \frac{1}{r}\int_0^r r\,\frac{\partial^2 V}{\partial s^2} dr dr,$$

and the right hand side is contracting with respect to r. Since we are only interested in cases in which $V(s,r)$ is expressed in DA, if $\partial^2 V/\partial s^2$ is nonzero, the integral $\int_0^r r\,\partial^2 V/\partial s^2 dr$ contains r to a positive power. Thus, the factor $1/r$ in the outer integral simply lowers the power of r by one, and the right hand side of the fixed point form can be evaluated in DA without posing trouble. To perform the DA fixed point iteration for the purpose of obtaining the full potential $V(s,r)$, one only needs to prepare the on-axis potential expression $V(s,r)|_{r=0}$ as the boundary condition.

4. Behavior of the Out-of-Plane Expansion for an Analytical Model

In order to assess the ability to utilize the high-order derivatives of the fields in the midplane within the above framework for an out-of-plane expansion, we study a representative example for which an analytical field representation in 3D exists. Specifically, we consider the magnetic field of an arrangement of two rectangular uniformly magnetized iron bars. The bars extend to infinity from the inner surfaces characterized by $y = \pm d$ parallel to the midplane, which is located at $y = 0$. We denote by $x_{1,2}$ and $z_{1,2}$ the horizontal coordinates of the four corners of the magnet, so that the magnetized material of the bars is located inside $x_1 \le x \le x_2$ and $z_1 \le z \le z_2$.

For this bar magnet one can obtain an analytic solution for the magnetic field $\vec{B}\,(x,y,z)$, see for example Refs. 14–16. The fields are given by

$$\begin{aligned}
B_y\,(x,y,z) &= \frac{B_0}{4\pi}\sum_{i,j}(-1)^{i+j}\left[\arctan\left(\frac{X_i\cdot Z_j}{Y_+\cdot R_{ij}^+}\right) + \arctan\left(\frac{X_i\cdot Z_j}{Y_-\cdot R_{ij}^-}\right)\right] \\
B_x\,(x,y,z) &= \frac{B_0}{4\pi}\sum_{i,j}(-1)^{i+j}\left[\ln\left(\frac{Z_j + R_{ij}^-}{Z_j + R_{ij}^+}\right)\right] \\
B_z\,(x,y,z) &= \frac{B_0}{4\pi}\sum_{i,j}(-1)^{i+j}\left[\ln\left(\frac{X_i + R_{ij}^-}{X_i + R_{ij}^+}\right)\right],
\end{aligned} \tag{2}$$

where $X_i = x - x_i$, $Y_\pm = d \pm y$, $Z_i = z - z_i$, and $R_{ij}^\pm = \left(X_i^2 + Z_j^2 + Y_\pm^2\right)^{\frac{1}{2}}$. The geometric layout and midplane field of such a magnet is shown in Fig. 3.

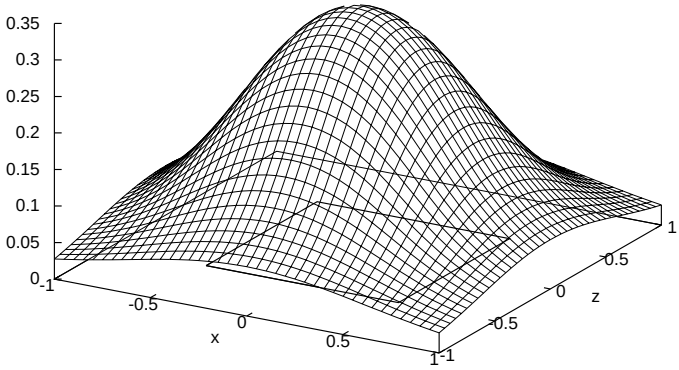

Fig. 3. The midplane field distribution of the bar magnets. The rectangular cross-section of the bars $[-0.5, 0.5] \times [-0.5, 0.5]$ is clearly marked on the graph.

This particular field arrangement can serve as useful test case for assessing the performance of computational methods. By itself, it represents a special case of the field of a magnetic dipole. But moreover, because the out-of-plane expansion schemes above are linear in the fields, it is also very indicative of the general behavior of any such methods, since most more complicated fields such as those in FFAGs are merely made by superimposing dipole-type fields of various apertures.

We next utilize the DA-based out-of-plane expansion method to determine the predicted field in space. Figure 4 shows the predicted fields at 25%, 50% and 75% of the aperture d. The left picture shows the vertical component B_y of the field, the middle picture shows B_x. The field component B_z is not shown directly since it is merely symmetric to B_x. The right picture shows the B_x and B_z components of the field as vectors for better clarity. The out-of-plane expansions were carried out to order 21.

It is quite apparent that the resulting field distributions are very smooth, suggesting the absence of major computational errors and inaccuracies. We now quantitatively analyze the quality of the out-of-plane expansion by a direct comparison with the true values of the field given by Eq. (2) and focus our attention to the dependence of the error on the expansion order that is being utilized. Furthermore, since the out-of-plane expansion is expected to lose accuracy with larger distance, we also study the quality of the expansion for distances to the midplane of $0.25d$, $0.5d$, and $0.75d$. For each computation order and distance from the plane, we evaluate the errors over a rectangular grid of 41×41 points for x and z in $[-1, +1]$.

We calculate both the average error of the representation as out-of-plane expansion, as well as its maximum. We record results for out-of-plane expansions of orders 3, 5, ..., 21 of the fields, corresponding to orders 4, 6, ..., 22 in the scalar potential. Since the field B_y is symmetric with respect to y, odd orders do not appear in its expansion with respect to y. Similarly, since the B_x and B_z fields are antisymmetric with respect to y, these fields do not exhibit even orders. So in order to show the trend of the accuracy with order, it is convenient to increase the orders by two in

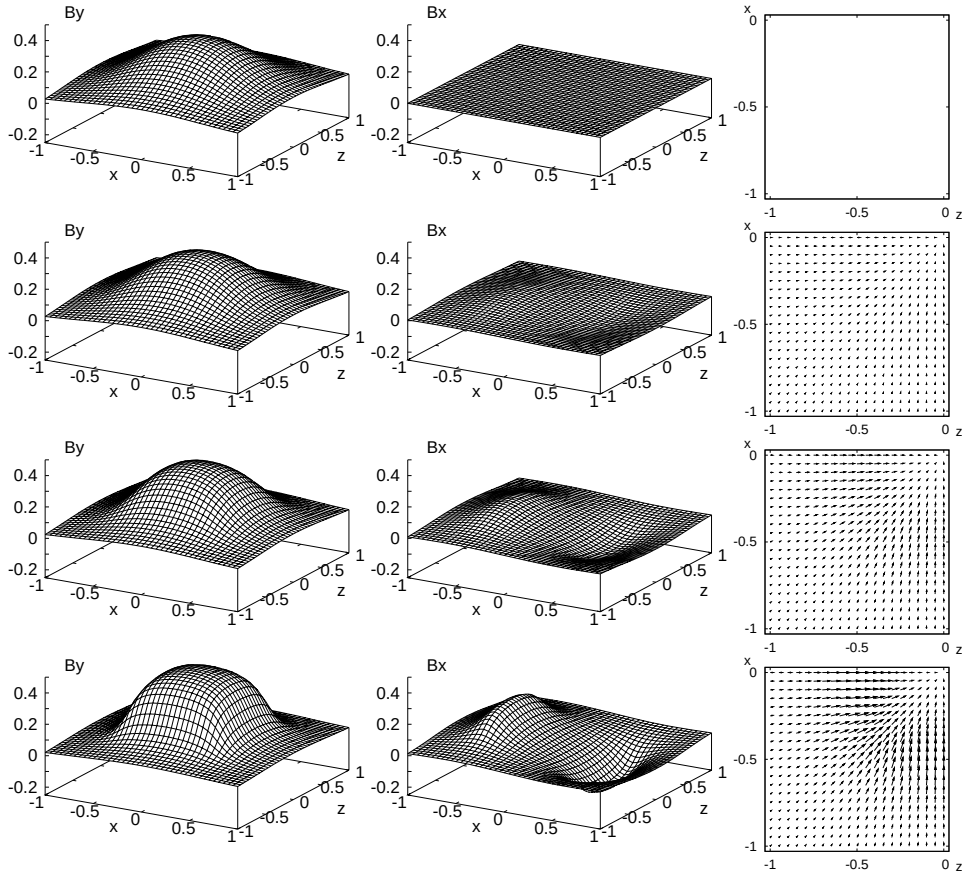

Fig. 4. Field distribution of the bar magnet in the x and y planes at $y = 0\%$ (midplane), 25%, 50%, and 75% of the half aperture d. The distributions of B_y and B_x are shown in 3D plots, and the B_x–B_z behavior is shown by vectors.

each step, and by choosing these orders to be odd, the actual highest appearing order of the B_y field is one order lower, while the highest appearing order for the B_x and B_z fields responsible for focusing effects is of the order shown.

Figure 5 shows a logarithmic plot for the resulting computational accuracies for the field component B_y. The other components are not shown since their behavior for each data point is within a few percent of those of B_y and thus lead to nearly indistinguishable plots. It can be seen that at the lowest order of 3 for B_x and B_z, the accuracies only range from about 10^{-3} to 10^{-1}, while at order 11 they reach 10^{-10} to 10^{-2}, and at order 21 they achieve 10^{-16} to 10^{-4}.

5. Out-of-Plane Expansion in Realistic FFAG Models

We now turn our attention to actual fields as they would appear in FFAG magnets. We utilize a field model based on superposition of individual combined function

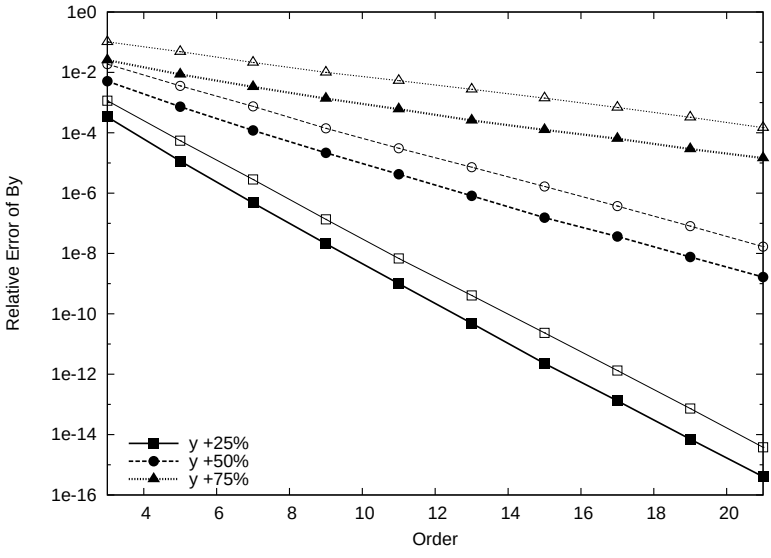

Fig. 5. Relative error of B_y of the bar magnet field depending on the out-of-plane expansion order at $y = 25\%$, 50%, 75% of the half aperture d as a function of the out-of-plane expansion order of the fields; the corresponding order of the potentials is higher by 1. The average error value (black markers) and the maximum error value (transparent markers) are plotted. Relative errors of B_x and B_z behave essentially the same way.

dipole fields as discussed in Ref. 17. Figure 6 shows the typical layout of such a FFAG ring, here made of nine individual cells, each of which contains two halves of a bending magnet (green) and a smaller magnet (red) bending in the opposite direction, both with a half aperture of 1 cm. The edges are carefully chosen so as to maintain horizontal and vertical tune stability.[18–20]

The fields are modeled utilizing an Enge falloff from the edges shown in the models, where the coefficients of the Enge function have been carefully adjusted to represent the situation of a permanent magnet, which constitutes one of the contemplated methods of constructing the magnet. Figure 7 shows the falloff of the resulting magnet on the right, and COSY's default fringe field falloff for dipoles on the left. Note that the FFAG falloff is steeper, leading to larger derivatives, and thus larger azimuthal out-of-plane field components.

As a result of the fringe fields thus imposed, the midplane field profile for B_y turns from the hard edge model shown in the leftmost picture of Fig. 8 to that shown in the rightmost one. For comparison, the softer falloff based on standard COSY dipoles is shown in the middle.

We now turn our attention to the performance of the DA-based out-of-plane expansion method described above and used in the code COSY. Figure 9 shows the predicted fields at 25%, 50% and 75% of the aperture d. The left picture shows the vertical component B_y of the field, the middle picture shows B_x. The right picture shows the B_x and B_z components of the field as vectors for better clarity.

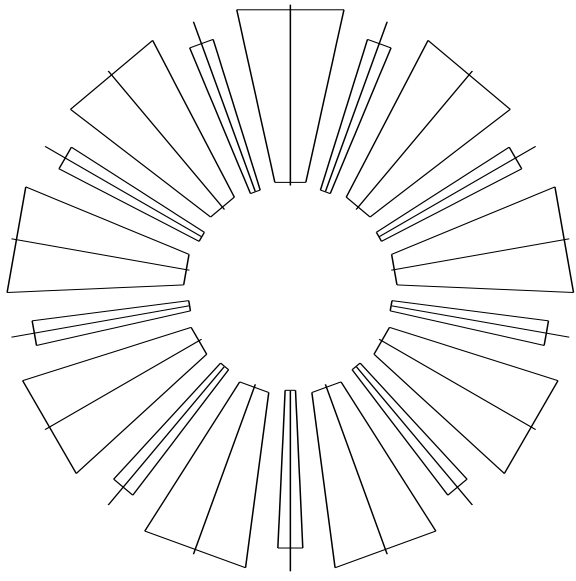

Fig. 6. Layout of a 9 cell model of non-scaling FFAG.

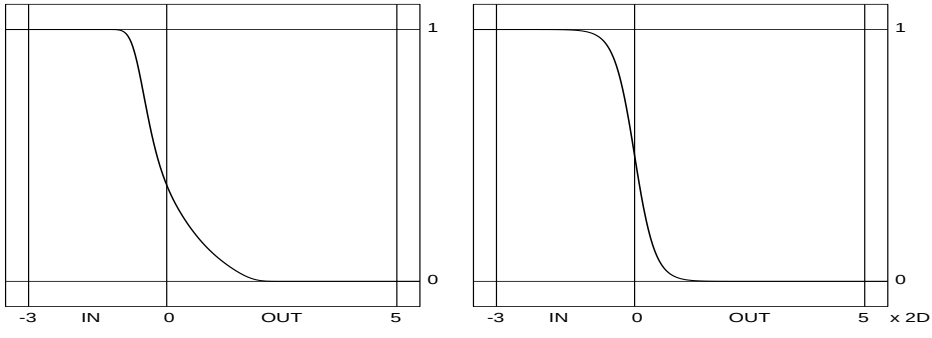

Fig. 7. Fringe field falloff profile based on Enge models. Left: default COSY dipole model, and right: model based on a permanent magnet, deemed more realistic for FFAG models.

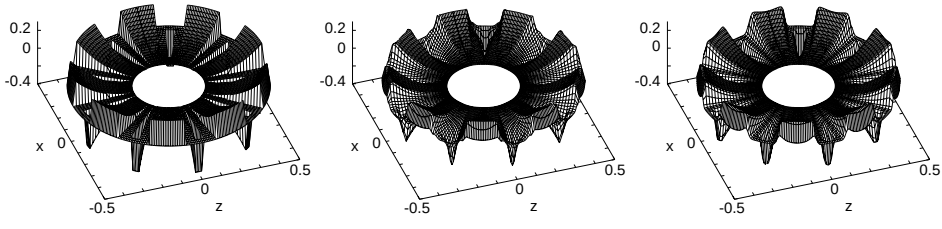

Fig. 8. Midplane field distribution of three FFAG models: A hard edge model, with fringe fields based on COSY default DI model, and with fringe field based on the field of permanent magnets as in the bar model.

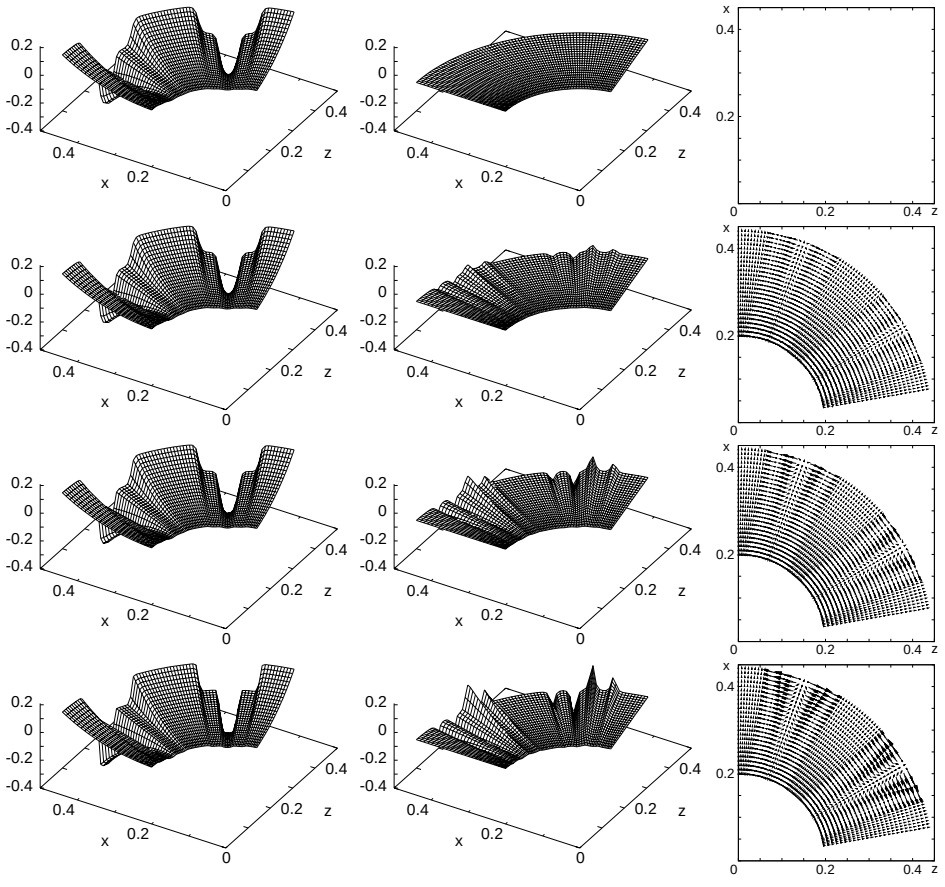

Fig. 9. Field distribution of a 80° section in the x and y planes—in the midplane and at $y =$ 2.5 mm, 5 mm, 7.5 mm planes. The distributions of B_y and B_θ are shown in 3D plots, and the B_r–B_θ behavior is shown by vectors. $0.20 \leq r \leq 0.44$ mm.

The out-of-plane expansions were carried out to order 21. It is apparent that the complexity of the resulting fields increases with larger distance to the midplane, and a rich amount of structure develops especially in the B_x field responsible for focusing.

We now quantitatively analyze the quality of the out-of-plane expansion. Different from the case of the bar magnet studied in the previous section, the exact value of the field is not known. So we perform our comparisons of accuracy of lower-order expansion by a comparison to an expansion of order 25 and assume that the differences with expansions of lower orders are meaningful estimates for the errors of these expansions. Again, since the out-of-plane expansion is expected to lose accuracy with larger distance, we also study the quality of the expansion for distances to the midplane of $0.25d$, $0.5d$, and $0.75d$. For each computation order and distance

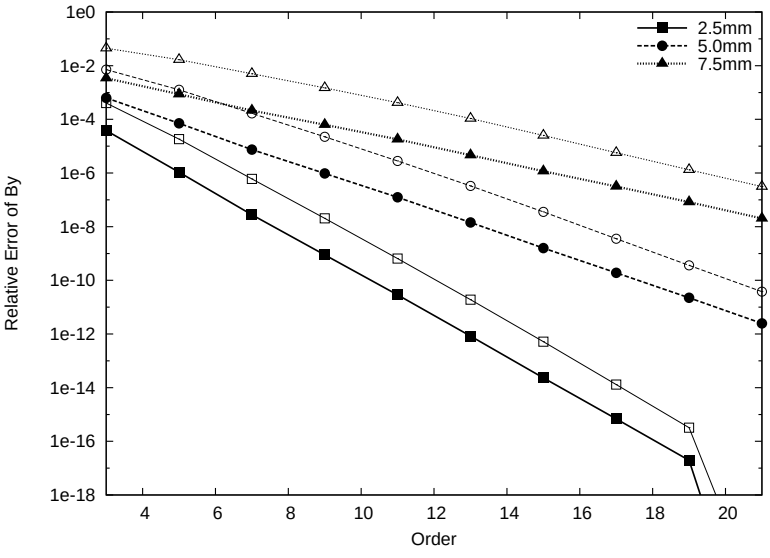

Fig. 10. Relative error of B_y depending on the out-of-plane expansion order at $y = 2.5$ mm, 5 mm, 7.5 mm planes. Shown are average error (black markers) and maximum error (transparent markers). The relative error of B_θ behaves almost identical, and the relative error of B_r is slightly lower but with the same overall behavior.

from the plane, we evaluate the errors over a grid in polar coordinates of 25×81 points in radius and azimuthal angle.

As before, we calculate both the average error of the representation as out-of-plane expansion, as well as its maximum. We record results for out-of-plane expansions of orders 3, 5, ..., 21 of the fields, corresponding to orders 4, 6, ..., 22 in the scalar potential. Since the field B_y is symmetric with respect to y, again odd orders do not appear in its expansion with respect to y, and likewise in B_x and B_z even orders do not appear.

Figure 10 shows a logarithmic plot for the resulting computational accuracies for the field component B_y. As before, the other components are not shown since their behavior for each data point is within a few percent of those of B_y and thus lead to nearly indistinguishable plots. It can be seen that at the lowest order of 3 for B_x and B_z, the accuracies only range from about 10^{-4} to 10^{-1}, while at order 11 they reach 10^{-11} to 10^{-3}, and at order 21 they achieve 10^{-16} to 10^{-6}.

To conclude, we see that for high-accuracy simulations, especially far away from the midplane, it is necessary to utilize rather high orders in the field expansions. While computations of tunes and related quantities require information only near the midplane, the study of detailed dynamics such as the computation of dynamic aperture limits requires careful consideration of all nonlinear effects including representations of high order.[17] Of particular consequence is the violation of the symplectic symmetry inherent in the dynamics in FFAGs, which arises whenever erroneous field representations are chosen.

Acknowledgments

The work was supported by the US Department of Energy and the National Science Foundation.

References

1. M. Berz. *Modern Map Methods in Particle Beam Physics*. Academic Press, San Diego, 1999. Also available at http://bt.pa.msu.edu/pub.
2. M. Berz. Differential algebraic description of beam dynamics to very high orders. *Particle Accelerators*, 24:109, 1989.
3. K. Makino, M. Berz, D. Errede, and C. J. Johnstone. High order map treatment of superimposed cavities, absorbers, and magnetic multipole and solenoid fields. *Nuclear Instruments and Methods A*, 519:162–174, 2004.
4. M. Berz. The new method of TPSA algebra for the description of beam dynamics to high orders. Technical Report AT-6:ATN-86-16, Los Alamos National Laboratory, 1986.
5. M. Berz. The method of power series tracking for the mathematical description of beam dynamics. *Nuclear Instruments and Methods*, A258:431–437, 1987.
6. K. Makino. *Rigorous Analysis of Nonlinear Motion in Particle Accelerators*. PhD thesis, Michigan State University, East Lansing, Michigan, USA, 1998. Also MSUCL-1093.
7. M. Berz and H. Wollnik. The program HAMILTON for the analytic solution of the equations of motion in particle optical systems through fifth order. *Nuclear Instruments and Methods*, A258:364–373, 1987.
8. K. Makino and M. Berz. Perturbative equations of motion and differential operators in nonplanar curvilinear coordinates. *International Journal of Applied Mathematics*, 3,4:421–440, 2000.
9. K. L. Brown, R. Belbeoch, and P. Bounin. First- and second- order magnetic optics matrix equations for the midplane of uniform-field wedge magnets. *Review of Scientific Instruments*, 35:481, 1964.
10. K. L. Brown. The ion optical program TRANSPORT. Technical Report 91, SLAC, 1979.
11. K. L. Brown. A first- and second-order matrix theory for the design of beam transport systems and charged particle spectrometers. Technical Report 75, SLAC, 1982.
12. M. Berz and K. Makino. COSY INFINITY Version 9.0 beam physics manual. Technical Report MSUHEP-060804, Department of Physics and Astronomy, Michigan State University, East Lansing, MI 48824, 2007. See also http://cosyinfinity.org.
13. M. Berz and K. Makino. COSY INFINITY Version 8.1 - user's guide and reference manual. Technical Report MSUHEP-20704, Department of Physics and Astronomy, Michigan State University, East Lansing, MI 48824, 2002. see also http://cosy.pa.msu.edu.
14. R. Degenhardt and M. Berz. High accuracy description of the fringe fields of particle spectrographs. In *Proceedings 1993 Particle Accelerator Conference*, Washington, DC, 1993.
15. R. Degenhardt and M. Berz. High accuracy description of the fringe field in particle spectrographs. *Nuclear Instruments and Methods*, A427:151–156, 1999.
16. S. L. Manikonda and M. Berz. An accurate high-order method to solve the Helmholtz boundary value problem for the 3D Laplace equation. *International Journal of Pure and Applied Mathematics*, 23,3:365–378, 2005.

17. K. Makino, M. Berz, P. Snopok, and C. Johnstone. High-order description of the dynamics in FFAGs and related accelerators. *International Journal Modern Physics A*, 24, 5:908–922, 2009.
18. Carol Johnstone and S. Koscielniak. *DPB Newsletter*, chapter The New Generation of FFAG Accelerators, pages 12–14. American Physical Society, 2008.
19. C. Johnstone, M. Berz, K. Makino, and P. Snopok. Innovations in fixed-field accelerators: Design and simulation. In *Proceedings, 19th International Conference on Cyclotrons and their Applications*, in print.
20. C. Johnstone, M. Berz, K. Makino, and P. Snopok. Isochronous (CW) non-scaling FFAGs: Design and simulation. In *Proceedings, 2010 Advanced Accelerator Concepts Workshop*, in print.